How to cite: *Angew. Chem. Int. Ed.* **2023**, *62*, e202307035
doi.org/10.1002/anie.202307035

Fused-Ring Systems

Anthracene-Porphyrin Nanoribbons

*He Zhu, Qiang Chen, Igor Rončević, Kirsten E. Christensen, and Harry L. Anderson**

Abstract: π-Conjugated nanoribbons attract interest because of their unusual electronic structures and charge-transport behavior. Here, we report the synthesis of a series of fully edge-fused porphyrin-anthracene oligomeric ribbons (dimer and trimer), together with a computational study of the corresponding infinite polymer. The porphyrin dimer and trimer were synthesized in high yield, via oxidative cyclodehydrogenation of singly linked precursors, using 2,3-dichloro-5,6-dicyano-1,4-benzoquinone (DDQ) and trifluoromethanesulfonic acid (TfOH). The crystal structure of the dimer shows that the central π-system is flat, with a slight S-shaped wave distortion at each porphyrin terminal. The extended π-conjugation causes a dramatic red-shift in the absorption spectra: the absorption maxima of the fused dimer and trimer appear at 1188 nm and 1642 nm, respectively (for the nickel complexes dissolved in toluene). The coordinated metal in the dimer was changed from Ni to Mg, using *p*-tolylmagnesium bromide, providing access to free-base and Zn complexes. These results open a versatile avenue to longer π-conjugated nanoribbons with integrated metalloporphyrin units.

The high charge-carrier mobilities and tunable band gaps of graphene nanoribbons (GNRs) make them promising materials for electronic and spintronic devices.[1,2] A simple example of a GNR is the 7-atom wide armchair ribbon **7-AGNR** (Figure 1a), which has a theoretical band gap of $E_g = 2.03$ eV (calculated with the HSE06 functional and in good agreement with experimental data).[3,4] The structural diversity of GNRs can be expanded by introducing heteroatoms,[5,6] and non-hexagonal aromatic rings.[7]

Edge-fused porphyrin nanoribbons (**P*N***, Figure 1b) stand out for their exceptionally narrow band gaps and high single-molecule conductances.[8,9] The calculated band gap for an infinitely long **P*N*** strand, with nickel(II) coordinated in every porphyrin, is $E_g = 0.34$ eV.[10] Furthermore, the properties of porphyrin-based materials can be tuned by coordination to almost every metal in the periodic table, providing a way to introduce paramagnetic spin centers or catalytic sites.[11]

Here we investigate a nanoribbon consisting of alternating edge-fused porphyrin and anthracene units, **AP*N*** (Figure 1c), which is a hybrid between **7-AGNR** and **P*N***. This hybrid ribbon has a calculated band gap of $E_g = 0.45$ eV, almost as narrow as that of **P*N***. The band structure calculations summarized in Figure 1 indicate that the effective masses of the charge carriers in the conduction band and valence band, m_{CB} and m_{VB}, for **AP*N*** and **P*N*** are exceptionally low, implying that these polymers should exhibit higher charge-carrier mobilities than **7-AGNR**.

Previously, porphyrin π-systems have been extended by fusion to a variety of aromatic units, including naphthalene,[12] anthracene,[13,14] pyrene,[15] perylene,[16] azulene[17] and other polycyclic aromatics.[18,19,20] In earlier work, we found it was essential to have an electron-donating ether substituent on the anthracene to promote oxidative fusion with a porphyrin.[13] This requirement made it impossible to fuse an anthracene bridge between two porphyrins. This impasse has now been overcome by using the improved reaction conditions for the Scholl reaction[21] pioneered by Rathore and co-workers,[14,18,22] in combination with nickel metalation of the porphyrins, so that they are not demetallated by the strongly acidic conditions. Another important feature of the porphyrin design is to use *meso*-aryl solubilizing substituents with *ortho*-methyl groups (e.g. mesityl) to prevent accidental oxidative fusion of the aryl group with the porphyrin (i.e. to prevent formation of a 5-membered ring).[18,23]

Synthesis of the anthracene-fused porphyrin dimers **AP2a** and **AP2b** (with mesityl and 2,6-dimethyl-4-dodecylphenyl aryl groups, respectively, Scheme 1) started with Suzuki–Miyaura coupling of the porphyrin boronate ester **1a**, **b** with 9,10-dibromoanthracene **2** to give **3a**,**b** in 54 % and 66 % yield, respectively. Swapping the boron and bromine functional groups in this Suzuki–Miyaura coupling (i.e. attempting to synthesize **3a**, **b** from the bromoporphyrin and the anthracene diboronic acid) was less successful due to formation of inseparable bis-anthryl linked porphyrin dimer by-products (see Supporting Information, Scheme S1, *Route 2*). Oxidative cyclodehydrogenation of **3a** and **3b** with

[*] H. Zhu, Dr. Q. Chen, Dr. I. Rončević, Dr. K. E. Christensen, Prof. H. L. Anderson
Department of Chemistry,
University of Oxford,
Chemistry Research Laboratory
OX1 3TA Oxford (UK)
E-mail: harry.anderson@chem.ox.ac.uk
Dr. I. Rončević
Institute of Organic Chemistry and Biochemistry of the Czech Academy of Sciences
Prague (Czech Republic)

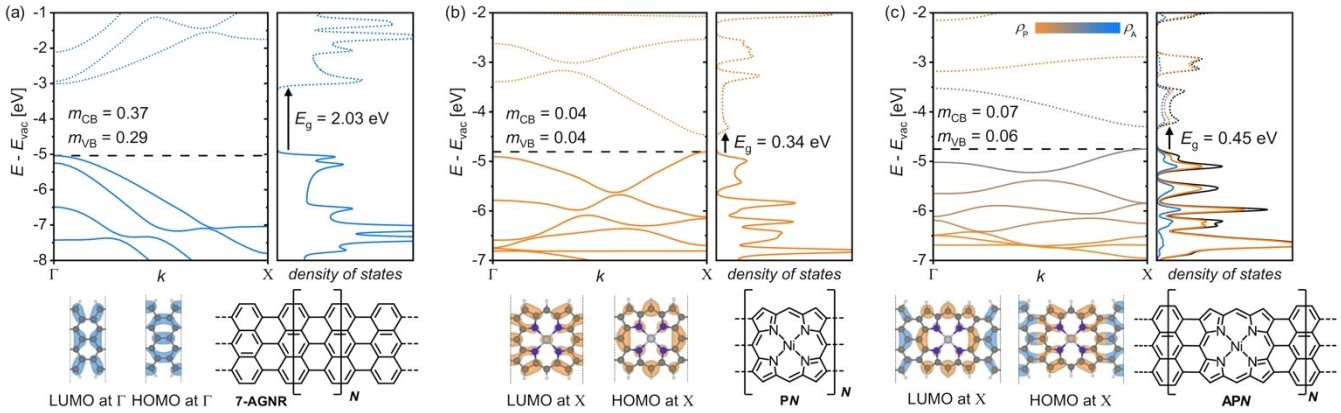

Figure 1. Band structures, density of states, and frontier orbitals plots of a) **7-AGNR**, b) ***PN*** and c) **APN**.[4] The band gap (E_g), valence and conductance band, and effective mass (m_{CB} and m_{VB}) are shown; energies are reported relative to the vacuum reference (E_{vac}). The color scale in the case of **APN** represents the proportion of electron density on anthracene (orange) or porphyrin (blue); occupied and unoccupied levels are shown by solid and dotted lines, respectively.

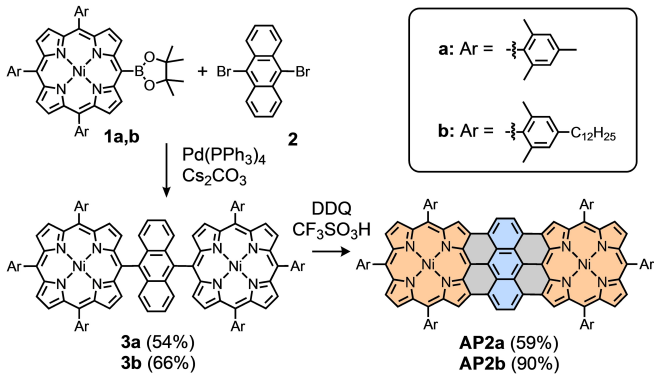

Scheme 1. Synthesis of **AP2a** and **AP2b**.

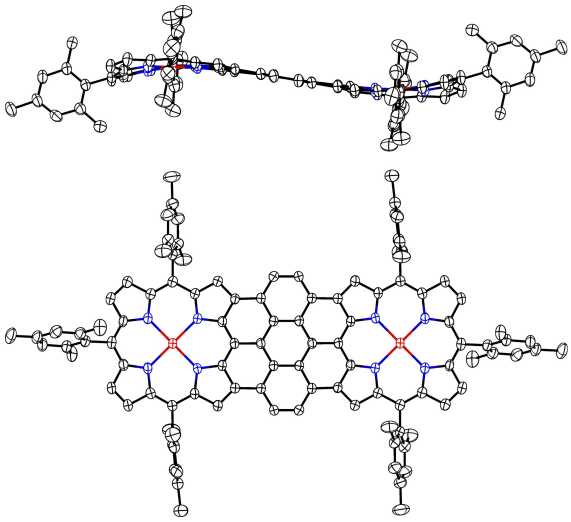

Figure 2. Side view (top) and front view (right) X-ray single-crystal structure of **AP2a**. Hydrogen atoms omitted for clarity. Thermal ellipsoids plotted at the 50% level.

2,3-dichloro-5,6-dicyano-1,4-benzoquinone (DDQ) and trifluoromethanesulfonic acid (CF_3SO_3H, TfOH) in dichloromethane (1:100, *v*/*v*)[18] gave the fully fused dimers **AP2a** (59%) and **AP2b** (90%).

The mesityl-substituted dimer **AP2a** is only soluble enough for NMR characterization in CS_2/CD_2Cl_2, whereas **AP2b** dissolves well in solvents such as dichloromethane and toluene. ^{1}H and ^{13}C NMR spectra of **AP2a** and **AP2b** recorded in the CS_2/CD_2Cl_2 (2:1, *v*/*v*) are well resolved and display the expected patterns of signals. The structure of **AP2a** was confirmed by single-crystal X-ray diffraction analysis of crystals grown by slow diffusion of ethanol vapor into a solution in CS_2/CD_2Cl_2 (Figure 2).[24] The central 24-atom coronene core of the dimer is essentially flat (root-mean-square deviation 0.039 Å), but the porphyrins bend away from this plane generating an S-shaped geometry. The nonplanar conformation of the porphyrin units (root-mean-square deviation of 24-atom core: 0.23 Å) is similar to that in many tetrasubstituted nickel(II) porphyrins, and is attributed to the small radius of the nickel(II) cation.[25] The molecular unit has a C_2 symmetry axis and the asymmetric unit contains one porphyrin and half the anthracene core. Molecules of **AP2a** pack into infinite linear strands with the mesityl group of one molecule making C–H/π-interactions with the next molecule in the chain (H···π distances: 2.63–3.35 Å; Figure S2).

The fully fused anthracene-linked porphyrin trimer was synthesized using the more soluble 2,6-dimethyl-4-dodecylphenyl-substituted porphyrins (Scheme 2). Suzuki–Miyaura coupling of **1b** with bisanthracenyl-porphyrin **4b** gave the singly linked precursor **5b** in 37% yield. Ring closure to **AP3b** was realized under the same Scholl reaction conditions in 81% yield. The well resolved MALDI-TOF mass spectrum of **AP3b** shows the expected molecular ion (Scheme 2, insert) and demonstrates that 16 H atoms are removed in the oxidative cyclodehydrogenation step. The ^{1}H NMR spectrum of **AP3b** (measured in CD_2Cl_2/CS_2; Figure S17) is consistent with the structure, although some peaks are poorly resolved and this compound was not soluble enough to recorded its ^{13}C NMR spectrum.

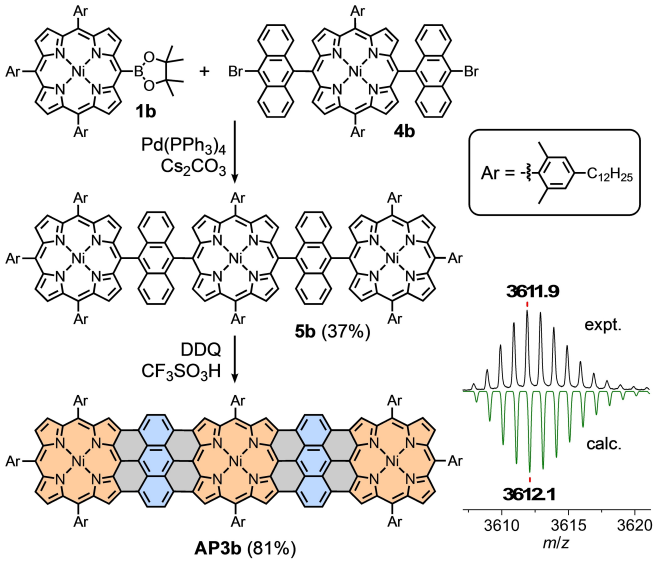

Scheme 2. Synthesis of **AP3b**. (Inset: experimental and calculated isotope patterns for the molecular ion of **AP3b** from MALDI-TOF MS.)

In order to evaluate the effect of the anthracene units on the electronic properties of these nanoribbons, we synthesized the directly edge-fused porphyrin dimer **P2b** and trimer **P3b** (Figure 3, see Supporting Information for synthesis), and compared their UV/Vis-NIR absorption spectra with those of **AP2b** and **AP3b** (Figure 4a; dimers in red; trimers in blue). The absorption spectra of **P2b** and **P3b** display typical features for edge-fused porphyrin oligomers, with Q bands at 874 nm and 1157 nm, respectively.[26] The incorporation of an anthracene bridge in **AP2b** results in a sharp intense absorption band at 1188 nm (optical gap 1.04 eV). The absorption maximum of **AP3b** shows a further red-shift to 1642 nm (optical gap 0.76 eV). Thus, **AP2b** and **AP3b** exhibit strongly red-shifted absorption spectra, compared with their counterparts without anthracene units, **P2b** and **P3b**, respectively. The absorption spectra of **AP2b** and **AP3b** are in good agreement with the calculated transitions from time-dependent DFT (TD-DFT) calculations using B3LYP functional (see Supporting Information, Figure S40).

Square-wave and cyclic voltammetry were used to compare the redox potentials of dimers **AP2b** and **P2b** (Figure 4b). The first oxidation and reduction potentials of **AP2b** are 0.07 and −0.78 V, respectively (vs. Fc/Fc^+), corresponding to an electrochemical gap of 0.85 eV. When compared to **P2b** (E_{ox} 0.26 V, E_{red} −1.14 V; E_g 1.40 eV), it is clear that fusing the bridging anthracene into center of the dimer makes **AP2b** easier to oxidize and reduce, resulting in a narrower HOMO–LUMO gap.

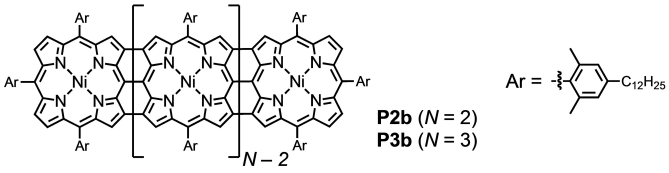

Figure 3. Structures of the directly edge-fused porphyrin dimer **P2b** and trimer **P3b**, which were synthesized for comparison with **AP2b** and **AP3b**.

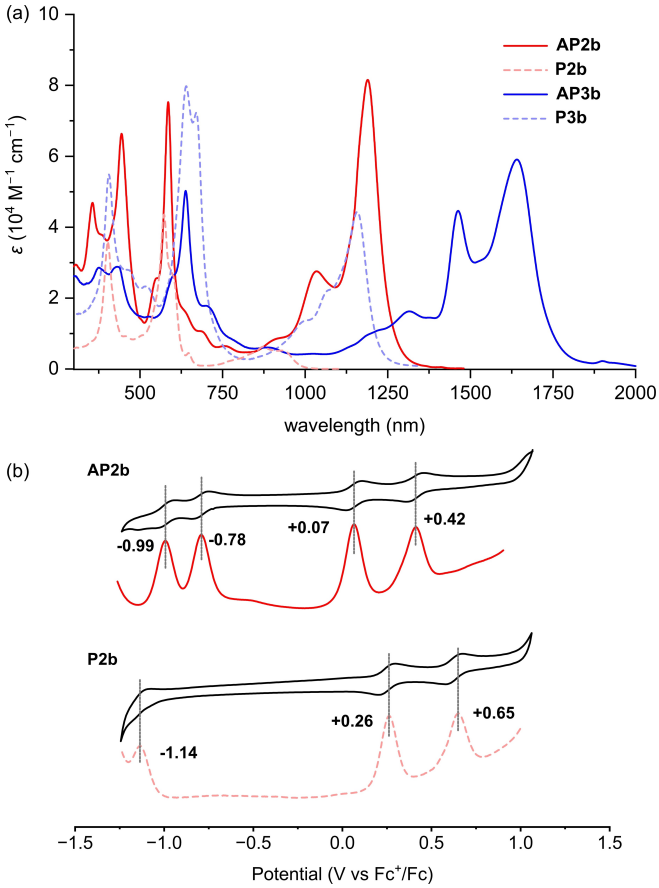

Figure 4. a) UV/Vis-NIR absorption spectra of **AP2b** and **AP3b** in comparison with the corresponding directly fused porphyrin dimer **P2b** and trimer **P3b** measured in toluene-d_8 at room temperature. b) Square-wave and cyclic voltammograms of **AP2b** and **P2b** in dichloromethane with 0.1 M NBu_4NPF_6 as electrolyte; potentials relative to internal ferrocene (Fc/Fc^+ at 0 V).

The coordination chemistry of porphyrins provides an opportunity to tune their electronic, photophysical, magnetic and catalytic behavior by changing the metal. We therefore investigated whether the coordinated Ni^{II} in anthracene-porphyrin nanoribbons could be changed for other metals using **AP2b** as a model compound. Many nickel(II) porphyrins can be demetallated by sulfuric acid in trifluoroacetic acid (TFA), but **AP2b** is inert to these strongly acidic conditions. Another approach to removing nickel from porphyrins is to use a Grignard reagent such as *p*-tolylmagnesium bromide, which exchanges Ni^{2+} for Mg^{2+}.[27] We found that treatment of **AP2b** with excess *p*-tolylmagnesium bromide at 80 °C affords the magnesium anthracene fused porphyrin dimer (**Mg-AP2b**, Scheme 3) in 90 % yield. This magnesium complex is readily demetallated with TFA to give the free-base **FB-AP2b** in 94 % yield, which can coordinate other metals; for example, reaction with zinc acetate gave **Zn-AP2b** in 96 % yield.

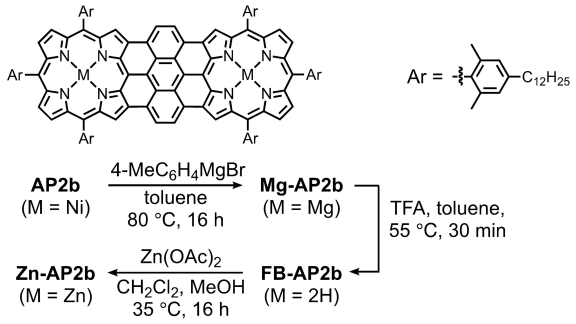

Scheme 3. Metal exchange from **AP2b** to prepare the magnesium (**Mg-AP2b**), free-base (**FB-AP2b**) and zinc (**Zn-AP2b**) porphyrin dimer.

In summary, we have reported the synthesis of a fully fused anthracene-bridged porphyrin dimers **AP2a**,**b** and trimer **AP3b**, via cyclodehydrogenation with DDQ/TfOH. The X-ray crystal structure of the dimer confirms that fusion creates a planar coronene core, although coordinated Ni^{II} results in some nonplanarity in the terminal porphyrins. These oligomers are models for one-dimensionally extended porphyrin-anthracene nanoribbons. Multi-metal systems are accessible via metal exchange, opening up an approach to diverse functional nanoribbons. The main challenge in synthesizing longer ribbons of this type will be to design an aryl sidechain that can maintain solubility, while being stable to strongly acidic and oxidizing conditions.

Acknowledgements

This work was supported by the ERC (grant 885606 ARO-MAT) and the European Community (MSCA project 101064401 ElDelPath). Q. C. is grateful to the German Research Foundation for a Walter Benjamin fellowship (grant number CH 2577/1-1). Computational resources were provided by the Cirrus UK National Tier-2 HPC Service at EPCC (http://www.cirrus.ac.uk) funded by the University of Edinburgh and EPSRC (EP/P020267/1), as well as the Ministry of Education, Youth and Sports of the Czech Republic through the e-INFRA CZ (ID : 90140).

Conflict of Interest

The authors declare no conflict of interest.

Data Availability Statement

The data that support the findings of this study are available in the Supporting Information of this article.

Keywords: Graphene Nanoribbons · Metal Exchange · NIR Absorption · Nanostructures · Porphyrinoids

[1] V. Saraswat, R. M. Jacobberger, M. S. Arnold, *ACS Nano* **2021**, *15*, 3674–3708.
[2] R. S. K. Houtsma, J. de la Rie, M. Stöhr, *Chem. Soc. Rev.* **2021**, *50*, 6541–6568.
[3] a) P. Ruffieux, J. Cai, N. C. Plumb, L. Patthey, D. Prezzi, A. Ferretti, E. Molinari, X. Feng, K. Müllen, C. A. Pignedoli, R. Fasel, *ACS Nano* **2012**, *6*, 6930–6935; b) S. Linden, D. Zhong, A. Timmer, N. Aghdassi, J. H. Franke, H. Zhang, X. Feng, K. Müllen, H. Fuchs, L. Chi, H. Zacharias, *Phys. Rev. Lett.* **2012**, *108*, 216801.
[4] Geometries were optimized using PBE-D2; this was followed by a single-point calculation using the HSE06 short-range screened hybrid functional, which has 25 % exact exchange in the short range and 0 % in the long range. Band structures were obtained by interpolating HSE06 results using Boltztrap2. Band energies are reported with respect to the vacuum reference. See Supporting Information for details.
[5] A. Borissov, Y. K. Maurya, L. Moshniaha, W.-S. Wong, M. Żyła-Karwowska, M. Stępien, *Chem. Rev.* **2022**, *122*, 565–788.
[6] a) S. Kawai, S. Nakatsuka, T. Hatakeyama, R. Pawlak, T. Meier, J. Tracey, E. Meyer, A. S. Foster, *Sci. Adv.* **2018**, *4*, eaar7181; b) J. Cai, C. A. Pignedoli, L. Talirz, P. Ruffieux, H. Söde, L. Liang, V. Meunier, R. Berger, R. Li, X. Feng, K. Müllen, R. Fasel, *Nat. Nanotechnol.* **2014**, *9*, 896–900; c) E. C. H. Wen, P. H. Jacobse, J. Jiang, Z. Wang, R. D. McCurdy, S. G. Louie, M. F. Crommie, F. R. Fischer, *J. Am. Chem. Soc.* **2022**, *144*, 13696–13703; d) F. Hernández-Culebras, M. Melle-Franco, A. Mateo-Alonso, *Angew. Chem. Int. Ed.* **2022**, *61*, e202205018.
[7] a) A. Narita, X.-Y. Wang, X. Feng, K. Müllen, *Chem. Soc. Rev.* **2015**, *44*, 6616–6643; b) M. Liu, M. Liu, L. She, Z. Zha, J. Pan, S. Li, T. Li, Y. He, Z. Cai, J. Wang, Y. Zheng, X. Qiu, D. Zhong, *Nat. Commun.* **2017**, *8*, 14924; c) J. Lee, A. J. Kalin, T. Yuan, M. Al-Hashimi, L. Fang, *Chem. Sci.* **2017**, *8*, 2503–2521; d) S. R. Bheemireddy, M. P. Hautzinger, T. Li, B. Lee, K. N. Plunkett, *J. Am. Chem. Soc.* **2017**, *139*, 5801–5807.
[8] a) A. Tsuda, A. Osuka, *Science* **2001**, *293*, 79–82; b) T. Ikeda, N. Aratani, A. Osuka, *Chem. Asian J.* **2009**, *4*, 1248–1256.
[9] E. Leary, B. Limburg, A. Alanazy, S. Sangtarash, I. Grace, K. Swada, L. J. Esdaile, M. Noori, M. T. González, G. Rubio-Bollinger, H. Sadeghi, A. Hodgson, N. Agraït, S. J. Higgins, C. J. Lambert, H. L. Anderson, R. J. Nichols, *J. Am. Chem. Soc.* **2018**, *140*, 12877–12883.
[10] The presence of the nickel(II) cation in **P*N*** significantly increases the band gap, compared with the corresponding zinc(II) complex; V. Posligua, A. Aziz, R. Haver, M. D. Peeks, H. L. Anderson, R. Grau-Crespo, *J. Phys. Chem. C* **2018**, *122*, 23790–23798. The smaller band gap of the zinc complex appears to be a consequence of its full $d(x^2\text{-}y^2)$ orbitals, which elevate the energy of the valence band.
[11] a) M. Jurow, A. E. Schuckman, J. D. Batteas, C. M. Drain, *Coord. Chem. Rev.* **2010**, *254*, 2297–2310; b) M. Urbani, M. Grätzel, M. K. Nazeeruddin, T. Torres, *Chem. Rev.* **2014**, *114*, 12330–12396; c) T. Tanaka, A. Osuka, *Chem. Soc. Rev.* **2015**, *44*, 943–969.
[12] a) A. N. Cammidge, P. J. Scaife, G. Berber, D. L. Hughes, *Org. Lett.* **2005**, *7*, 3413–3416; b) M. Tanaka, S. Hayashi, S. Eu, T. Umeyama, Y. Matano, H. Imahori, *Chem. Commun.* **2007**, 2069–2071.
[13] a) N. K. S. Davis, M. Pawlicki, H. L. Anderson, *Org. Lett.* **2008**, *10*, 3945–3947; b) N. K. S. Davis, A. L. Thompson, H. L. Anderson, *Org. Lett.* **2010**, *12*, 2124–2127; c) N. K. S. Davis, A. L. Thompson, H. L. Anderson, *J. Am. Chem. Soc.* **2011**, *133*, 30–31.
[14] P. Zhang, C. Yu, Y. Yin, J. Droste, S. Klabunde, M. R. Hansen, Y. Mai, *Chem. Eur. J.* **2020**, *26*, 16497–16503.

[15] O. Yamane, K. I. Sugiura, H. Miyasaka, K. Nakamura, T. Fujimoto, K. Nakamura, T. Kaneda, Y. Sakata, M. Yamashita, *Chem. Lett.* **2004**, *33*, 40–41.
[16] a) C. Jiao, K.-W. Huang, Z. Guan, Q.-H. Xu, J. Wu, *Org. Lett.* **2010**, *12*, 4046–4049; b) C. Jiao, K.-W. Huang, C. Chi, J. Wu, *J. Org. Chem.* **2011**, *76*, 661–664.
[17] K. Kurotobi, K. S. Kim, S. B. Noh, D. Kim, A. Osuka, *Angew. Chem. Int. Ed.* **2006**, *45*, 3944–3947.
[18] a) Q. Chen, L. Brambilla, L. Daukiya, K. S. Mali, S. De Feyter, M. Tommasini, K. Müllen, A. Narita, *Angew. Chem. Int. Ed.* **2018**, *57*, 11233–11237; b) Q. Chen, A. Lodi, H. Zhang, A. Gee, H. Wang, F. Kong, M. Clarke, M. Edmondson, J. Hart, J. O'Shea, W. Stawski, J. Baugh, A. Narita, A. Saywell, M. Bonn, K. Müllen, L. Bogani, H. L. Anderson, *ChemRxiv Preprint* **2023**, https://doi.org/10.26434/chemrxiv-2023-ghvdb.
[19] J. P. Lewtak, D. T. Gryko, *Chem. Commun.* **2012**, *48*, 10069–10086.
[20] H. Mori, T. Tanaka, A. Osuka, *J. Mater. Chem. C* **2013**, *1*, 2500–2519.
[21] a) M. Grzybowski, K. Skonieczny, H. Butenschçn, D. T. Gryko, *Angew. Chem. Int. Ed.* **2013**, *52*, 9900–9930; b) Y. Zhang, H. Pun, Q. Miao, *Chem. Rev.* **2022**, *122*, 14554–14593.
[22] a) L. Zhai, R. Shukla, R. Rathore, *Org. Lett.* **2009**, *11*, 3474–3477; b) L. Zhai, R. Shukla, S. H. Wadumethrige, R. Rathore, *J. Org. Chem.* **2010**, *75*, 4748–4760.
[23] a) J. H. Heo, T. Ikeda, J. M. Lim, N. Aratani, A. Osuka, D. Kim, *J. Phys. Chem. B* **2010**, *114*, 14528–14536; b) N. Fukui, S.-K. Lee, K. Kato, D. Shimizu, T. Tanaka, S. Lee, H. Yorimitsu, D. Kim, A. Osuka, *Chem. Sci.* **2016**, *7*, 4059–4066; c) M. M. Martin, C. Oleszak, F. Hampel, N. Jux, *Eur. J. Org. Chem.* **2020**, 6758–6762.
[24] Single-crystal X-ray diffraction data were collected at 150 K using a (Rigaku) Oxford Diffraction SuperNova diffractometer and CrysAlisPro. Structure was solved using "Superflip" [a) L. Palatinus, G. Chapuis, *J. Appl. Crystallogr.* **2007**, *40*, 786) before refinement with CRYSTALS b) P. Parois, R. I. Cooper, A. L. Thompson, *Chem. Cent. J.* **2015**, *9*, 30; c) R. I. Cooper, A. L. Thompson, D. J. Watkin, *J. Appl. Crystallogr.* **2010**, *43*, 1100] as per the Supporting Information (CIF). Deposition Number 2244225 contains the supplementary crystallographic data for this paper. These data are provided free of charge by the joint Cambridge Crystallographic Data Centre and Fachinformationszentrum Karlsruhe Access Structures service.
[25] C. J. Kingsbury, M. O. Senge, *Coord. Chem. Rev.* **2021**, *431*, 213760.
[26] a) A. Tsuda, H. Furuta, A. Osuka, *J. Am. Chem. Soc.* **2001**, *123*, 10304–10321; b) A. K. Sahoo, Y. Nakamura, N. Aratani, K. S. Kim, S. B. Noh, H. Shinokubo, D. Kim, A. Osuka, *Org. Lett.* **2006**, *8*, 4141–4144; c) D. Kim, A. Osuka, *J. Phys. Chem. A* **2003**, *107*, 8791–8816.
[27] K. Murakami, Y. Yamamoto, H. Yorimitsu, A. Osuka, *Chem. Eur. J.* **2013**, *19*, 9123–9126.

Manuscript received: May 19, 2023
Accepted manuscript online: June 9, 2023
Version of record online: June 23, 2023